09

Formation of arrays of dynamic microcavities in a three-level medium

© M.V. Arkhipov, R.M. Arkhipov, N.N. Rosanov

Ioffe Institute, St. Petersburg, Russia

e-mail: mikhail.v.arkhipov@gmail.com, arkhipovrostislav@gmail.com, nnrosanov@mail.ru

Received August 07, 2025
Revised August 07, 2025
Accepted September 05, 2025

The previously predicted phenomenon of the formation of localized arrays of dynamic microresonators (DM) in a three-level resonant medium is theoretically studied. The effect occurs during an asymmetric (relative to the center of the medium) collision of two or three single-cycle, attosecond pulses, similar in action to 2π-pulses of self-induced transparency. It is shown that this effect, initially discovered in a two-level medium, is also preserved in three-level systems with different level configurations, which indicates its universality. The possibility of controlling the spatial configuration of microresonators by varying the time delay between pulses is established. The results open new prospects for ultrafast optics, attosecond physics, and topological photonics, including the creation of petahertz switches and control of light localization.

Keywords: extremely short pulses, attosecond pulses, dynamic microcavities, topological photonics, time-dependent media.

DOI: 10.61011/EOS.2025.09.62306.8463-25

Introduction

High-Q optical microcavities and waveguide structures [1–6] play a key role in modern photonics and quantum optics, finding applications in the development of compact laser sources [7], studies of exciton polaritons [8], and topological photonics [4,9,10]. Systems with spatially modulated parameters, demonstrating topological mode protection [11–14] and unusual light localization modes [15–17], are of particular interest. However, such stationary structures have a fundamental limitation the inability to dynamically control their parameters on ultrafast (single-cycle and sub-cycle) time scales.

A promising area to overcome this limitation is time-varying media [{]18 where rapid changes in the refractive index lead to new effects: temporal reflection and refraction of waves [19,20], dynamic light localization [21], and thresholdless laser generation [22]. However, in most works, the control of such media is carried out with multi-cycle femtosecond laser pulses [23], which does not allow reaching the shortest time scales.

Advances in attosecond pulse generation [24–26] have opened the possibility to study electronic processes on the time scale of the electron orbital period in the Bohr orbit. The relevance of research in this area is confirmed by the awarding of the Nobel Prize in Physics for studies conducted in this field [27]. Especially interesting are ultrashort pulses (USP) containing one or fewer oscillations of the light field [28–30]. Such pulses enable ultrafast control of quantum systems [31] and hold promise for petahertz electronics [32].

Interaction of USP with resonant media recently predicted a number of nonlinear effects impossible with multi-cycle pulses, see reviews [33,34] and monograph [35]. Among them are pulse self-compression [36], light self-stopping [37], and formation of dynamic microcavities (DM) [38–40] (see also reviews [41–43] and cited literature). In particular, symmetric collision of USP in a resonant medium creates isolated high-Q DM [38–40], capable of effectively trapping light [37].

In [44] an asymmetric with respect to the medium center weak half-cycle pulses (propagating in the medium not in self-induced transparency (SIT) regime) were studied. This work showed the possibility to induce regions in the medium with nearly constant population difference in the pulse overlap region and Bragg population gratings forming on both sides of the overlap region filling the entire medium.

It was recently discovered that under ***asymmetric*** collision of single-cycle 2π-like SIT pulses, a ***ordered array*** of two or more DM localized exclusively in the pulse overlap region forms in a two-level medium [45]. However, real media are multi-level, and the resonator configurations may significantly change. This makes the study of DM dynamics in multi-level systems relevant, which has not yet been addressed.

In this paper, based on numerical solution of Maxwell-Bloch equations, the formation of DM arrays under asymmetric collision of single-cycle SIT pulses in a three-level medium is studied in detail for the first time. It is shown that the effect is universal and manifests in various level configurations. It was established that the spatial distribution of microcavities can be controlled by the time delay between pulses.

The results are important for ultrafast optics where DM arrays can be used to create petahertz switches and modulators. In attosecond physics, such structures open new possibilities to control processes on times shorter than the light field oscillation period. In topological photonics, DM

arrays can be used to control light localization. Moreover, this phenomenon is interesting for petahertz electronics requiring signal control at extremely high frequencies.

Results for the two-level medium model

Before discussing these effects in a multi-level medium, key results for the two-level medium are briefly reproduced [45] to establish basic phenomena, then detailed investigation in the three-level medium follows. This approach reveals the universality of the effect, analyzes preservation of DM array formation with complicated energy level structure, and compares resonator dynamics in different level configurations.

Special attention is paid to how additional transitions in the three-level system affect the shape and properties of formed DM compared to the two-level case. Note that results presented here for the two-level system, although qualitatively similar [45], are obtained for other parameters and serve as an important basis for comparison with the three-level case, constituting the main novelty of this study.

The model used in this section is based on the Maxwell-Bloch equation system describing light pulse interaction with a resonant medium. This system includes: the equation for the off-diagonal density matrix element ρ_{12} describing coherent polarization of the medium$P(z,t)$, the equation for population difference (inversion) $n = \rho_{11} - \rho_{22}$, where ρ_{11} and ρ_{22} represent populations of the lower and upper levels respectively. Also, a one-dimensional wave equation for the electric field strength$E(z,t)$ describing light pulse propagation in the medium [46]:

$$\frac{\partial \rho_{12}(z,t)}{\partial t} = -\frac{\rho_{12}(z,t)}{T_2} + i\omega_0\rho_{12}(z,t) - \frac{i}{\hbar} d_{12}E(z,t)n(z,t), \quad (1)$$

$$\frac{\partial n(z,t)}{\partial t} = -\frac{n(z,t) - n_0(z)}{T_1} + \frac{4}{\hbar} d_{12}E(z,t)\mathrm{Im}\rho_{12}(z,t), \quad (2)$$

$$P(z,t) = 2N_0 d_{12}\mathrm{Re}\rho_{12}(z,t), \quad (3)$$

$$\frac{\partial^2 E(z,t)}{\partial z^2} - \frac{1}{c^2}\frac{\partial^2 E(z,t)}{\partial t^2} = \frac{4\pi}{c^2}\frac{\partial^2 P(z,t)}{\partial t^2}. \quad (4)$$

The considered equation system (1)–(4) contains the following parameters: $\hbar$ the reduced Planck constant, t — time, z — longitudinal coordinate,c — the speed of light in vacuum, P — medium polarization, d_{12} — the transition dipole moment, ω_0 — the transition frequency ($\lambda_0 = 2\pi c/\omega_0$ — the transition wavelength), N_0 — the concentration of two-level particles, n_0 — the population difference of the medium in absence of electric field ($n_0 = 1$ for absorbing medium). The density matrix equation system (1)–(3) was solved by the 4th-order Runge-Kutta method, and the wave equation (4) — by finite differences [47].

Numerous experimental and theoretical studies confirm the presence of coherent effects predicted by this model, including Rabi oscillations of atomic populations [48–50]. In particular, the predicted in low-level models effect of atomic population grating formation induced by ultrashort pulses is observed even under partial ionization of the medium, confirmed by numerical solution of the Schrödinger equation [51]. The adequacy of low-level models to describe ultrashort pulse propagation in resonant media has been discussed in detail in [38–43].

The model considers only homogeneous broadening of the quantum transition of the medium. Direct numerical results show that main features of coherent ultrashort pulse propagation in the medium, obtained without inhomogeneous broadening, are preserved when including it [52]. Inhomogeneous broadening can possibly be suppressed by trapping the atomic assembly at cryogenic temperatures [53], Stark effect application [54], quantum dot cooling [55], and other methods described in a large body of literature. These circumstances allow disregarding inhomogeneous broadening further.

Numerical simulations send series of counter-propagating single-cycle pulses from vacuum into the medium, consisting of two half-waves of opposite polarity (Fig. 1). The number of pulses varies, so they collide multiple times in the medium. The two-level medium is located between coordinates $z = 2\lambda_0$ and $z = 10\lambda_0$ (vacuum outside the medium region). The simulation domain length was $L = 12\lambda_0$. Before pulse arrival, the medium field is absent and medium is in the ground state. The expression for pulses traveling left to right (pulses $i = 1, 3, 5$ etc., Fig. 1) at $z = 0$ is

$$E(t) = E_0 \sum_i e^{-\frac{(t-\Delta_i)^2}{\tau^2}} \sin[\omega_0(t-\Delta_i)]. \quad (5)$$

Pulses traveling opposite direction (even numbered $j = 2, 4, 6\ldots$, Fig. 1) are defined by a similar expression at $z = L$:

$$E(t) = E_0 \sum_j e^{-\frac{(t-\Delta_j)^2}{\tau^2}} \sin[\omega_0(t-\Delta_j)]. \quad (6)$$

Here, Δ_i, Δ_j -are delays chosen so that pulses collide asymmetrically in the medium. Delay values for the first two pulses *1* and *2*, Δ_1, Δ_2 are listed in Table 1. Parameters of the two-level medium (wavelength λ_0 of the transition $1 \to 2$ and transition dipole moment d_{12}), pulse amplitude, and duration are given in Table 1. Such parameters (transition wavelengths in the hundreds of nanometers, dipole moments of a few Debye, etc.) are realized in a wide class of media, e.g., atomic vapors, gases, and others (see discussion below).

Pulse field amplitude and duration were chosen so that pulses act similarly to 2π-self-induced transparency (SIT) pulses. In this case, the first half-wave of the field transfers the medium from the ground to the excited state, and the second half-wave returns it to the ground state [56]. Such pulses with durations of hundreds of attoseconds can be obtained experimentally [28].

Table 1. Parameters used in numerical simulations in the two-level medium

Frequency (wavelength λ_0) of transition $1 \to 2$	$\omega_{12} = 1.55 \cdot 10^{16}$ rad/s ($\lambda_{12} = \lambda_0 = 121.6$ nm)
Dipole moment of the transition $1 \to 2$	$d_{12} = 3.27$ D
Concentration of atoms	$N_0 = 10^{20}$ cm^{-3}
Field amplitude	$E_{01} = 5.7 \cdot 10^6$ ESU
Parameter τ	$\tau = 200$ as
Delays Δ_1, Δ_2	$\Delta_1 = 2.5\tau$
	$\Delta_2 = 8\tau$
Population difference relaxation time and medium polarization	$T_1 - T_2 = 1$ ns

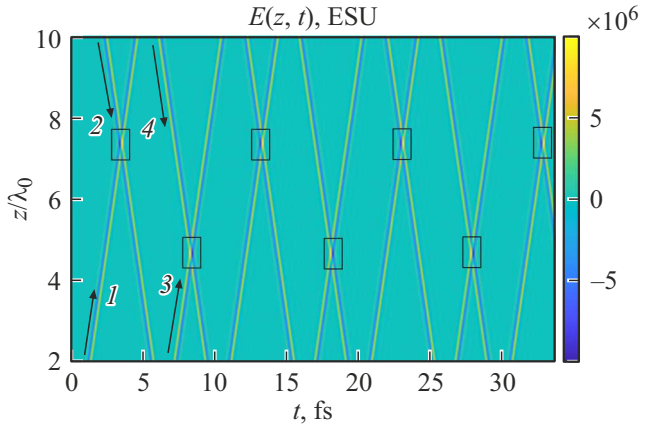

Figure 1. (coloured online). Scheme of pulse propagation in the medium. The first 4 pulses are marked by numbers. The directions of pulse propagation are shown by arrows. Each collision occurs near the points $z_{c1} \sim 4.3\lambda_0$ and $z_{c1} \sim 7.7\lambda_0$. The rectangles highlight these areas.

Numerical results in two-level medium

Numerical results are shown for the two-level medium in Fig. 1–3. Similar results were obtained earlier in the two-level medium in [45] but for a different delay parameter Δ_2. Parameters of this calculation are given in Table 1. We briefly discuss numerical results for the two-level medium below as they are needed for the study of DM in the three-level medium.

Fig. 1 illustrates pulse field strength and their collision moments at different points of the medium. Figs. 2 and 3 show spatiotemporal dynamics of population difference $n = \rho_{11} - \rho_{22}$ and medium polarization $P(z, t)$, respectively. Numerical results in Fig. 2 show the formation of a pair of DM localized near points $z = 4\lambda_0$ and $z = 8\lambda_0$, their shape changing after each collision between pulses.

The observed spatial distribution of population difference (Fig. 2) demonstrates characteristic features of a dynamic microcavity (DM), where the central region corresponds to full return of the medium to the ground state ($n = 1$), while edge regions form a Bragg grating with a sub-

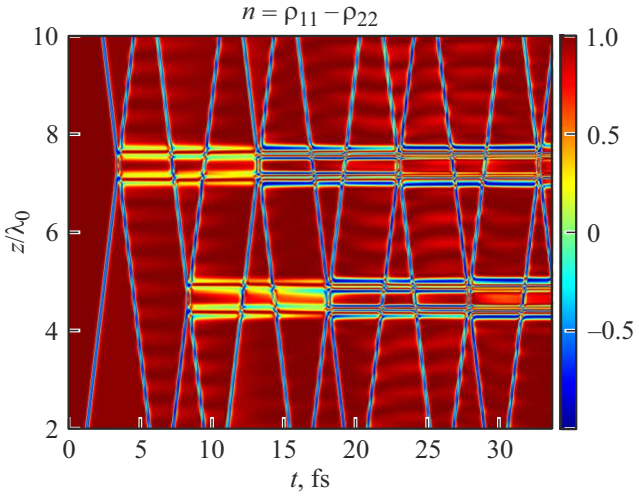

Figure 2. (coloured online). Spatiotemporal dynamics of population difference $\rho_{11} - \rho_{22}$ in two-level medium.

wavelength modulation period. Quantitative analysis of the spatial frequency of this structure reveals its progressive increase with successive pulse collisions, with the upper DM ($z \approx 7.7\lambda_0$) showing the most significant growth after the third and fourth collisions, and the lower DM after the fourth and fifth interactions.

In this case, the structure period is much smaller than the transition wavelength, approximately $\lambda_0/10$. Note this small period is explained by all population difference changes occurring in ultranarrow spatial regions in the pulse overlap zone, much smaller than the transition wavelength. This approach allows lattices with arbitrarily small period, not only with spatial periods multiple of even numbers of transition wavelengths ($\lambda_0/2, \lambda_0/4 \ldots$), as was the case when pulses did not overlap in the medium [57].

A fundamental difference from the previously studied symmetric collision case [39] is the formation of DM pairs localized in different medium regions under an asymmetric interaction configuration. The key feature is precise control of such structures' parameters by managing conditions of multiple pulse collisions in the resonant medium.

The physical nature of the observed phenomenon is related to the coherent interaction of pulses with the medium operating in the mode where pulse duration τ and time delays between them Δ are much shorter than polarization relaxation time T_2 ($\tau, \Delta \ll T_2$). Similar population grating formation processes are known for ultrashort pulses [57–60] and multi-cycle pulses [61–63], but the fundamental difference here is that it can only be implemented for ultrashort pulses enabling ultrafast medium excitation.

An important aspect is the nonlinear polarization dynamics showing complex spatiotemporal behavior (Fig. 3), where each successive pulse coherently controls oscillations leading to the formation of a specific population distribution. Correlation between DM localization and spatial polariza-

tion distribution confirms their interrelation and key role in forming resonant structures.

Critical parameters for effect realization are strict adherence to single-cycle SIT pulse condition 2πsatisfaction of time scale relations $\tau \ll T_2$ and maintaining optimal medium density [40]. Early studies [44] confirm relaxation of these conditions (departure from SIT mode) leads to effect disappearance. The observed DM array formation phenomenon is a new physical effect predicted earlier in [45], opening perspectives for light field control methods in topological photonics and ultrafast optical device creation. Further study of electromagnetic wave propagation in such structures requires separate consideration, while results of computational modeling in the three-level medium below confirm the universal nature of the described phenomena.

Emergence of dynamic microcavity array in three-level medium

The above results raise the question of these structures' formation in multilevel media. The physical mechanism forming these structures obviously remains in multilevel media (applicability of few-level models for such problems was justified, e.g., in [40–43]). Indeed, passing through a multilevel medium, pulses leave after them medium coherence oscillations i.e., oscillations of off-diagonal density matrix elements on each resonant transition of the multilevel medium, existing on timescales of order T_2. Each subsequent pulse acts on these oscillations either to stop or enhance them, leading to dynamic population difference gratings *on each resonant transition* of such media. The shape of these structures may vary depending on specific transition parameters, but the key fact is effect retention.

It is important to note these medium coherence oscillations persist even under partial medium ionization. Even if the first USP causes full ionization, by adjusting delay between successive pulses, ionization can be suppressed efficiently by the second pulse. This is confirmed by direct numerical Schrödinger equation solutions shown in [51]. Thus, ionization consideration does not cause effect disappearance, underscoring their robustness and justifying use of few-level models.

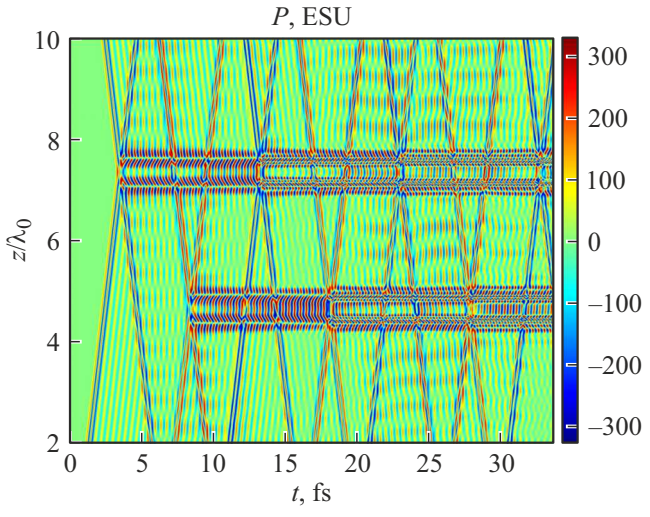

Figure 3. (coloured online). Spatiotemporal dynamics of polarization in two-level medium $P(z,t)$.

This is illustrated by the example of a three-level medium. The numerical model here is based on density matrix equations of the three-level medium combined with the wave equation. It includes equations for off-diagonal density matrix elements of the three-level medium $\rho_{21}, \rho_{32}, \rho_{31}$, equations for diagonal elements $\rho_{11}, \rho_{22}, \rho_{33}$, representing populations of 1st, 2nd, and 3rd states respectively, and the medium polarization equation $P(z,t)$ [46]:

$$\frac{\partial}{\partial t}\rho_{21} = -\rho_{21}/T_{21} - i\omega_{12}\rho_{21} - i\frac{d_{12}}{\hbar}E(\rho_{22}-\rho_{11}) - i\frac{d_{13}}{\hbar}E\rho_{23} + i\frac{d_{23}}{\hbar}E\rho_{31}, \quad (7)$$

$$\frac{\partial}{\partial t}\rho_{32} = -\rho_{32}/T_{32} - i\omega_{32}\rho_{32} - i\frac{d_{23}}{\hbar}E(\rho_{33}-\rho_{22}) - i\frac{d_{12}}{\hbar}E\rho_{31} + i\frac{d_{13}}{\hbar}E\rho_{21}, \quad (8)$$

$$\frac{\partial}{\partial t}\rho_{31} = -\rho_{31}/T_{31} - i\omega_{31}\rho_{31} - i\frac{d_{13}}{\hbar}E(\rho_{33}-\rho_{11}) - i\frac{d_{12}}{\hbar}E\rho_{32} + i\frac{d_{23}}{\hbar}E\rho_{21}, \quad (9)$$

$$\frac{\partial}{\partial t}\rho_{11} = \frac{\rho_{22}}{T_{12}} + \frac{\rho_{33}}{T_{13}} - \frac{\rho_{22}}{T_{122}} - \frac{\rho_{33}}{T_{133}} + i\frac{d_{12}}{\hbar}E(\rho_{21}-\rho_{21}^*) - i\frac{d_{13}}{\hbar}E(\rho_{13}-\rho_{13}^*), \quad (10)$$

$$\frac{\partial}{\partial t}\rho_{22} = -\frac{\rho_{22}}{T_{22}} + \frac{\rho_{11}}{T_{12}} + \frac{\rho_{33}}{T_{13}} - i\frac{d_{12}}{\hbar}E(\rho_{21}-\rho_{21}^*) - i\frac{d_{23}}{\hbar}E(\rho_{23}-\rho_{23}^*), \quad (11)$$

$$\frac{\partial}{\partial t}\rho_{33} = -\frac{\rho_{33}}{T_{33}} + \frac{\rho_{11}}{T_{13}} + \frac{\rho_{22}}{T_{23}} + i\frac{d_{13}}{\hbar}E(\rho_{13}-\rho_{13}^*) + i\frac{d_{23}}{\hbar}E(\rho_{23}-\rho_{23}^*), \quad (12)$$

$$P(z,t) = 2N_0 d_{12}\mathrm{Re}\rho_{12}(z,t) + 2N_0 d_{13}\mathrm{Re}\rho_{13}(z,t) + 2N_0 d_{23}\mathrm{Re}\rho_{23}(z,t). \quad (13)$$

Here, d_{12}, d_{13}, d_{23} are dipole moment matrix elements of transitions, $\omega_{12}, \omega_{13}, \omega_{23}$ are transition frequencies, T_{122}, T_{133}, T_{ik} are relaxation times. Parameter values are listed in Table 2. Pulse field parameters remain the same as in the previous section. Pulses (5), (6) collide in the medium at the same times and points as in Fig. 1.

Fig. 4–6 shows the population difference dynamics for each transition in the three-level medium. Unlike the two-level system, the three-level medium exhibits formation of

Table 2. Parameters of the three-level medium used in numerical calculations

Frequency (wavelengthλ_0) of transition $1 \rightarrow 2$	$\omega_{12} = 1.55 \cdot 10^{16}$ rad/s ($\lambda_{12} = \lambda_0 = 121.6$ nm)
Dipole moment of the transition $1 \rightarrow 2$	$d_{12} = 3.27$ D
Frequency (wavelength) of transition $1 \rightarrow 3$	$\omega_{13} = 1.84 \cdot 10^{16}$ rad/s ($\lambda_{13} = 102.6$ nm)
Dipole moment of the transition $1 \rightarrow 3$	$d_{13} = 5$ D
Frequency (wavelength) of transition $2 \rightarrow 3$	$\omega_{23} = 2.87 \cdot 10^{15}$ rad/s ($\lambda_{23} = 656.6$ nm)
Dipole moment of the transition $2 \rightarrow 3$	$d_{23} = 0$ D
Delays Δ_1, Δ_2	$\Delta_1 = 2.5\tau$ $\Delta_2 = 9.5\tau$
Relaxation times	$T_{ik} = 1$ ns $T_{122} = T_{133} = \infty$
Concentration of atoms	$N_0 = 10^{20}$ cm^{-3}

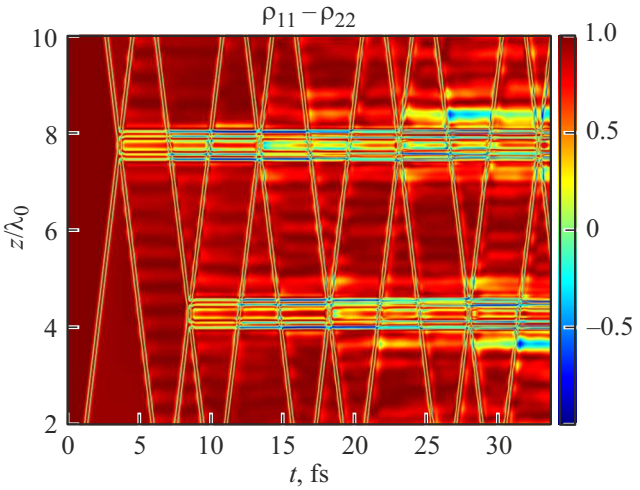

Figure 4. Spatiotemporal dynamics of the $\rho_{11} - \rho_{22}$ population difference of the three-level medium. The calculation parameters are listed in Table 2.

pairs arrays of dynamic microcavities (DM) localized on each resonant transition. This is a fundamentally new phenomenon absent in two-level systems, where dynamic modulations occur only on one transition. The medium polarization behavior shown in Fig. 7 also demonstrates significant differences. Calculations were performed for parameters given in Table 2, where the transition dipole moment is $d_{23} = 0$.

The key difference is that complete polarization oscillations in the three-level medium are determined by multiple transition frequencies, while only one frequency exists in the two-level system. This leads to a more complex dynamic modulation structure, clearly visible in Fig. 7. In particular, polarization oscillations in the three-level medium have a significantly more complex form than in the two-level case due to coherence oscillations on all transitions, resulting in

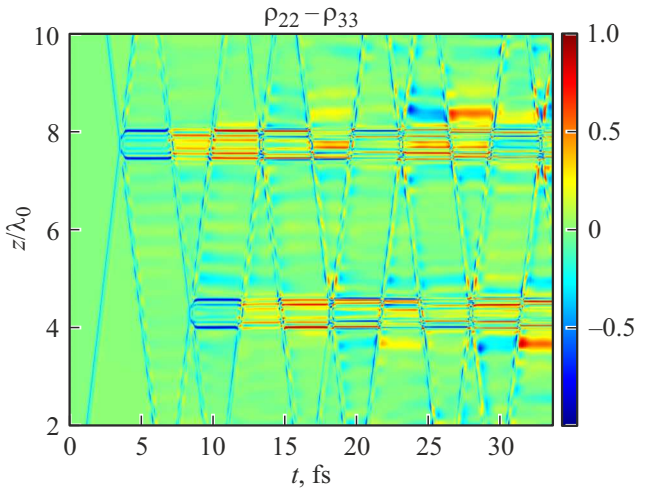

Figure 5. Spatiotemporal dynamics of the $\rho_{22} - \rho_{33}$ population difference of the three-level medium. The calculation parameters are listed in Table 2.

multiple frequency superposition and a more complicated overall pattern. In contrast, the two-level medium with a single resonant transition has relatively simple oscillation shapes.

Novelty of the results is also in the nature of localized oscillations. In the three-level medium (Fig. 7), polarization oscillations concentrate near points $z \sim 4\lambda_0$ and $z \sim 8\lambda_0$, where dynamic resonator arrays form. Their form becomes more complex, highlighting the multilevel medium structure's influence on system dynamics. This opens new possibilities to analyze and control dynamic modulations in complex quantum systems.

Thus, correlated localized oscillations of polarization and population difference coexist in the medium, leading to the formation of structures that act as microcavities. Such structures can trap light [37], potentially causing complete light stoppage and forming a bound oscillating field-matter structure called a stationary oscillaton. The properties of these structures were detailed in [37]. However, in [37] a quasi-resonator formed from a single pulse during its coherent propagation in a dense medium. In our case, resonator formation results from a pulse pair collision, representing a fundamentally different mechanism and emphasizing the novelty of obtained results.

The next case, shown in Fig. 8–10, was calculated for conditions when the transition dipole moment is $d_{13} = 0$, and $d_{23} = 0.5$ D. Other parameters are the same as the ones shown in Table 2. Analysis shows arrays of localized dynamic microcavities form here as well, but their shape differs somewhat from that in the three-level medium with $d_{23} = 0$.

Fig. 8–10 shows induced structures in this scheme are less diffuse compared to Fig. 4–6, more resembling structures in the two-level medium (Fig. 2). Notably, Fig. 8, illustrating inversion behavior on transition *1–2* shows spatial frequency increase of induced Bragg gratings

after the third and fourth pulse collisions for the upper DM localized near $z \sim 8\lambda_0$.

Thus, consideration of additional medium levels and level configuration changes do not eliminate the DM array formation effect predicted earlier for two-level media (Figs. 2, 3 and [45]). The influence of additional levels only slightly modifies the DM array shape, underscoring this effect's robustness to medium structure variations.

Formation of DM arrays under three-pulse excitation of the three-level medium

Previously, the formation of a DM pair under two-pulse excitation of two- and three-level media was considered. Earlier in [45], the possibility to create an array of three DM by adding a third pulse was shown. We demonstrate formation of this array in the three-level medium. Here, after pulses (6) from right to left, an additional pulse series in the form

$$E(z = L, t) = E_0 \sum_m e^{-\frac{(t-\Delta_m)^2}{\tau^2}} \sin[\omega_0(t - \Delta_m)]. \qquad (14)$$

The delay between pulse *2* from series (6) and the first pulse from this series (14) was $\Delta_{23} = 23\tau$. Spatial behavior of population difference on various transitions, with $d_{13} = 0$, $d_{23} = 0.5\,\mathrm{D}$ is shown in Figs. 11, 12. Arrays of complex structures form on different medium transitions, similarly to the two-level medium case analyzed in [45]. More complex structures arise at$d_{13} = 5\,\mathrm{D}$, $d_{32} = 0\,\mathrm{D}$ (Figs. 13, 14). but the DM formation effect persists.

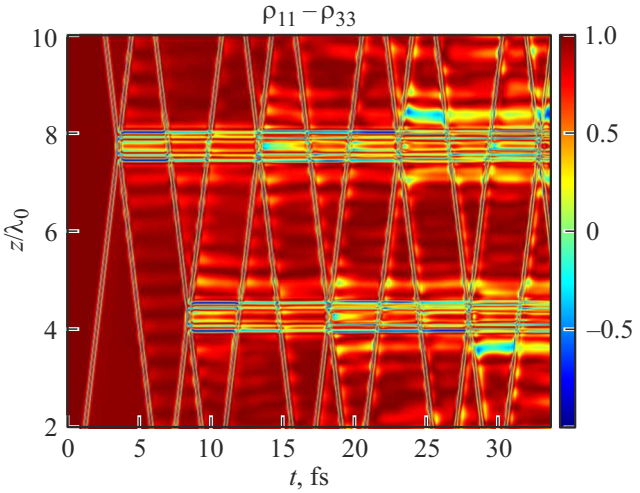

Figure 6. Spatiotemporal dynamics of the $\rho_{11} - \rho_{33}$ population difference of the three-level medium. The calculation parameters are listed in Table 2.

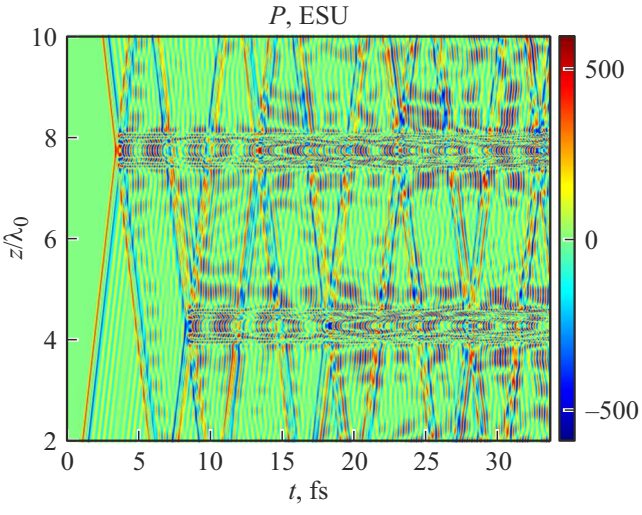

Figure 7. Spatiotemporal dynamics of polarization of a three-level medium $P(z, t)$.

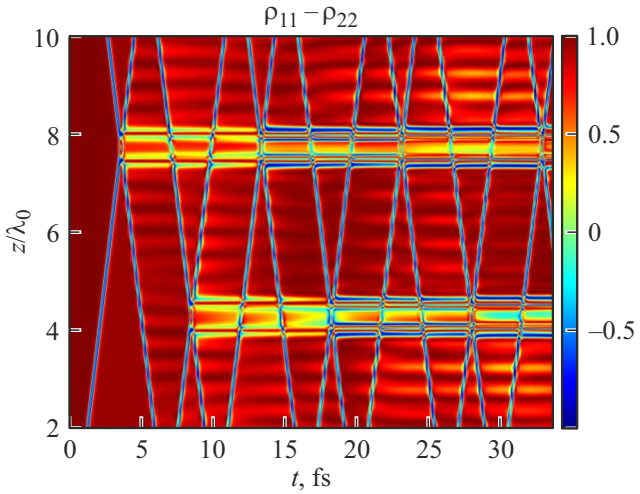

Figure 8. Spatiotemporal dynamics of the $\rho_{11} - \rho_{22}$ population difference of the three-level medium. $d_{13} = 0$, $d_{23} = 0.5\,\mathrm{D}$. Other parameters are the same as in Table 2.

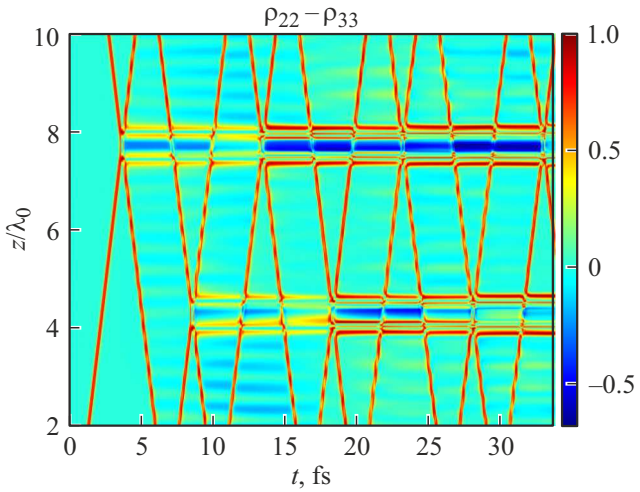

Figure 9. Spatiotemporal dynamics of the $\rho_{22} - \rho_{33}$ population difference of the three-level medium. $d_{13} = 0$, $d_{23} = 0.5\,\mathrm{D}$. Other parameters are the same as in Table 2.

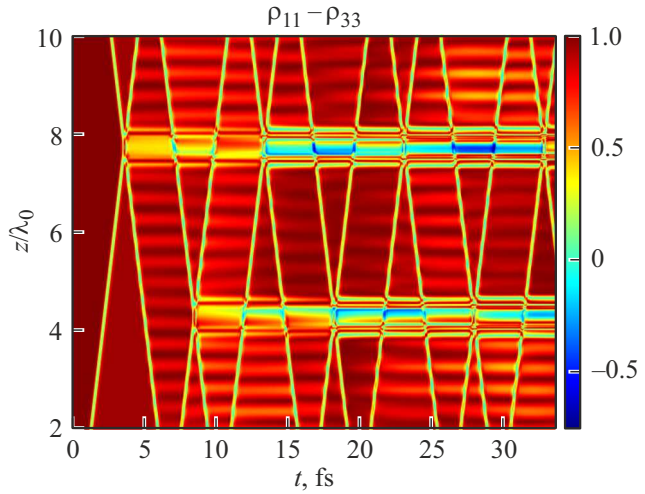

Figure 10. Spatiotemporal dynamics of the $\rho_{11} - \rho_{33}$ population difference of the three-level medium. $d_{13} = 0$, $d_{23} = 0.5$ D. Other parameters are the same as in Table 2.

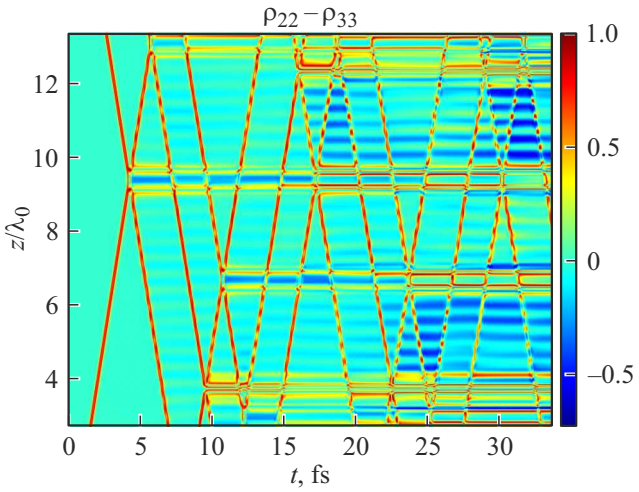

Figure 12. Spatiotemporal dynamics of the $\rho_{22} - \rho_{33}$ population difference of the three-level medium. $d_{13} = 0$, $d_{23} = 0.5$ D. Other parameters are the same as in Table 2.

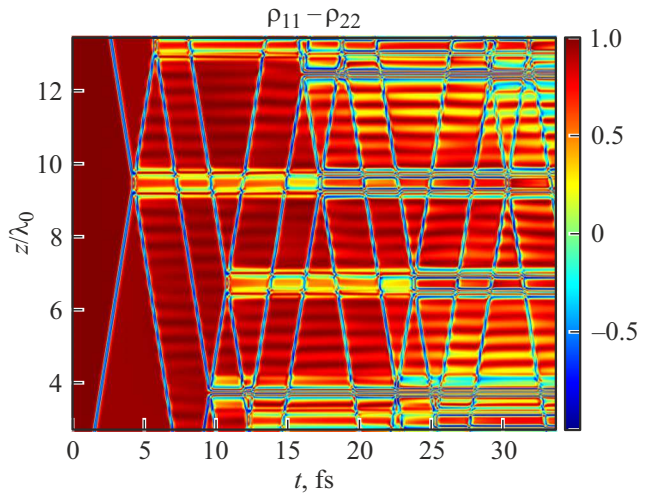

Figure 11. Spatiotemporal dynamics of the $\rho_{11} - \rho_{22}$ population difference of the three-level medium. $d_{13} = 0$, $d_{23} = 0.5$ D. Other parameters are the same as in Table 2.

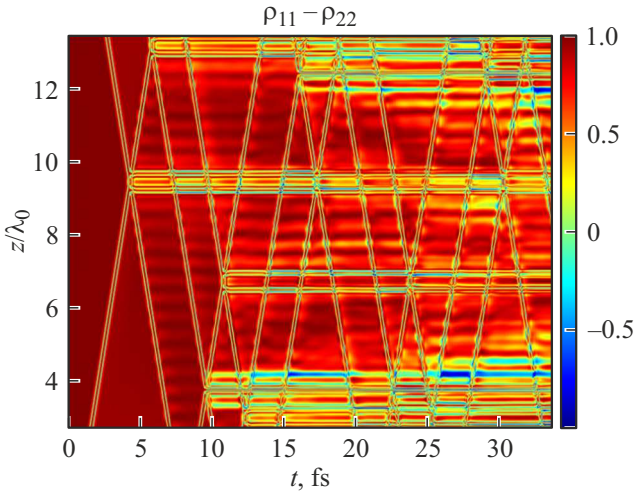

Figure 13. Spatiotemporal dynamics of population difference $\rho_{11} - \rho_{22}$ for a three-level medium. $d_{13} = 5$ D, $d_{32} = 0$ D. Other parameters are the same as in Table 2.

Discussion of experimental implementation of the effect

Formation of dynamic modulation arrays (DM) on each transition of multilevel media, where transition frequencies span various spectral ranges, opens wide application prospects in topological photonics. This allows control of radiation propagation from visible to ultraviolet (UV) and infrared (IR) ranges. Observed effects can be seen in media with large phase memory times T_2. including gases, quantum dots at low temperatures [55], crystals with rare-earth ions [64], and various two-dimensional materials such as 2D semiconductors [65] and twisted graphene [66], where exciton states with discrete hydrogen-like spectra exist, similar to the studied three-level medium. In these materials, exciton states with a discrete hydrogen-like spectrum are realized, similar to the one considered above for the three-level medium.

Moreover, an advanced research direction is the use of modern materials with pronounced discrete energy levels. Promising materials include transition metal dichalcogenides (TMDC) like MoS_2, WS_2 and WSe_2 exhibiting strong exciton effects and discrete energy levels ideal for observing such phenomena [67]. Heterostructures based on 2D materials such as borophene and phosphorene, possessing unique electronic and optical properties, are also of interest [68].

Additionally, perovskite nanocrystals and quantum dots based on them, like $CsPbBr_3$ demonstrate high coherence and discrete energy levels, opening new quantum optics research opportunities [69]. Moreover, a promising direction

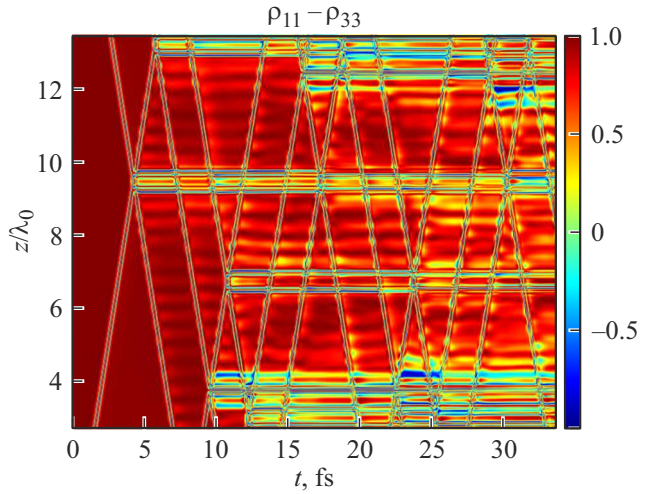

Figure 14. Spatiotemporal dynamics of the $\rho_{11} - \rho_{33}$ population difference of the three-level medium. $d_{13} = 5$ D, $d_{32} = 0$ D. Other parameters are the same as in Table 2.

is the use of nanostructured media consisting of metals and dielectrics. Nanostructured media composed of metals and dielectrics synthesized with modern methods [70–72] further expand experimental possibilities and practical applications.

Previous experimental observations of coherent effects such as Rabi oscillations in complex multilevel systems induced by few-cycle pulses in semiconductors [48], helium atoms [49]. and others support the feasibility of practical implementation. Increasing the number of pulses may lead to irregular DM arrays [73].

Conclusion

The presented work uses numerical modeling based on density matrix and wave equations to study in detail the formation of localized dynamic microresonator arrays under sequences of 2π-like single-cycle attosecond self-induced transparency pulses in two- and three-level resonant media. The observed effect is fundamentally non-stationary and occurs only for ultrashort pulses, impossible with multicycle pulse excitations.

The universality of dynamic microcavity formation is shown, preserved when transitioning from two-level to three-level systems with various level configurations. In particular, three-pulse excitation of a three-level medium forms arrays of three dynamic microcavities, with spatial configuration depending on level scheme type while maintaining fundamental dynamic properties.

The results obtained above may be applied in ultrafast optics and light pulse control methods. In particular, the studied effects are of interest for studying localization of light in complex media and attosecond switching. This work contributes to understanding nonlinear dynamics of ultrashort pulses in resonant systems and points to further research directions including radiation propagation features in such structures.

Funding

The research was supported by the Russian Science Foundation project 23-12-00012 (numerical modeling of DM in three-level media) and by the State Assignment of the Ioffe Institute of Physics and Technology, topic 0040-2019-0017 (numerical modeling of DM in two-level media).

Conflict of interest

The authors declare that they have no conflict of interest.

References

[1] K.J. Vahala. Nature, **424**, 839 (2003).
[2] H. Cao, J. Wiersig. Rev. Mod. Phys., **87**, 61 (2015).
[3] A. Pasquazi, M. Peccianti, L. Razzari, D.J. Moss, S. Coen, M. Erkintalo, Y.K. Chembo, T. Hansso et al. Phys. Rep., **729**, 1–81 (2018).
[4] H. Yu, X. Liu, W. Sun, Y. Xu, X. Liu, Y. Liu. Opt. & Laser Technol., **177**, 111099 (2024).
[5] Y. Sun, J. Wu, M. Tan, X. Xu, Y. Li, R. Morandotti, A. Mitchell, D.J. Moss. Adv. Opt. Photon., **15** (1), 86–175 (2023).
[6] E.A. Anashkina, M.P. Marisova, A.N. Osipov, A.V. Yulin, A.V. Andrianov. IEEE J. Sel. Top. Quantum. Electron., **30** (5), Art no. 2900208 (2024).
[7] L. Zhang, J. Hu, J. Wu, R. Su, Z. Chen, Q. Xiong, H. Deng. Progress in Quantum Electronics, **83**, 100399 (2022).
[8] J.P. Reithmaier, G. Sęk, A. Löffler, C. Hofmann, S. Kuhn, S. Reitzenstein, L.V. Keldysh, V.D. Kulakovskii, T.L. Reinecke, A. Forchel. Nature, **432**, 197–200550 (2004).
[9] V.V. Klimov. Phys. Usp., **66**, 263–287 (2023).
[10] I.L. Garanovich, S. Longhi, A.A. Sukhorukov, Y.S. Kivshar. Phys. Rep., **518**, 1–79 (2012).
[11] D. Smirnova, D. Leykam, Y. Chong, Y. Kivshar. Appl. Phys. Rev., **7**, 021306 (2020).
[12] L. Lu, J.D. Joannopoulos, M. Soljačić. Nature Photonics, **8** (11), 821–829 (2014).
[13] A.B. Khanikaev, G. Shvets. Nature Photonics, **11** (12), 763–773 (2017).
[14] T. Ozawa, H.M. Price, N. Goldman, O. Zilberberg, I. Carusotto. Rev. Mod. Phys., **91** (1), 015006 (2019).
[15] M. Segev, Y. Silberberg, D.N. Christodoulides. Nature Photonics, **7** (3), 197–204 (2013).
[16] T. Schwartz, G. Bartal, S. Fishman, M. Segev. Nature, **446**, 52 (2007).
[17] S. Mittal, J. Fan A. Migdall, J.M. Taylor. Nature Photonics, **7** (12), 1001–1005 (2013).
[18] T.T. Koutserimpas, F. Monticone. Opt. Mater. Express., **14**, 1222–1236712 (2024).
[19] T.T. Koutserimpas, R. Fleury. IEEE Trans. Antennas Propag., **68** (9), 6717–6724 (2020).
[20] S. Ramaccia, A. Toscano, F. Bilotti. Opt. Lett., **45** (20), 5836–5839 (2020).

[21] Y. Sharabi, E. Lustig, M. Segev. Phys. Rev. Lett., **126** (16), 163902 (2021).
[22] M. Lyubarov, Y. Lumer, A. Dikopoltsev E. Lustig, Y. Sharabi, M. Segev. Science, **377**, 425–428 (2022).
[23] E. Lustig, O. Segal, S. Saha, E. Bordo, S.N. Chowdhury, Y. Sharabi, A. Fleischer, A. Boltasseva, O. Cohen, V.M. Shalaev, M. Segeev. Nanophotonics, **12**, 1 (2023).
[24] F. Krausz. Rev. Mod. Phys., **96**, 030502 (2024).
[25] P. Agostini. Rev. Mod. Phys., **96**, 030501 (2024).
[26] A. L'Huillier. Rev. Mod. Phys., **96**, 030503 (2024).
[27] https://www.nobelprize.org/prizes/physics/2023/summary/
[28] M.T. Hassan, T.T. Luu, A. Moulet, O. Raskazovskaya, P. Zhokhov, M. Garg, N. Karpowicz, A.M. Zheltikov, V. Pervak, F. Krausz, E. Goulielmakis. Nature, **530**, 66 (2016).
[29] N. Rosanov, D. Tumakov, M. Arkhipov, R. Arkhipov. Phys. Rev. A, **104** (6), 063101 (2021).
[30] R.M. Arkhipov, M.V. Arkhipov, N.N. Rosanov. Quant. Electron., **50** (9), 801 (2020).
[31] M.T. Hassan. ACS Photonics, **11**, 334 (2024).
[32] C. Heide, P.D. Keathley, M.F. Kling. Nat. Rev. Phys., **6**, 648 (2024).
[33] N.N. Rosanov, M.V. Arkhipov, R.M. Arkhipov, A.V. Pakhomov. Contemporary Physics, **64** (3), 224 (2023).
[34] N.N. Rosanov, M.V. Arkhipov, R.M. Arkhipov. Phys. Usp., **67** (11), 1129 (2024).
[35] N.N. Rozanov, M.V. Arhipov, R.M. Arhipov. it Teragercovaya fotonika, pod red. V.Ya. Panchenko, A.P. Shkurinov (RAN, M., 2023), s. 360–393.
[36] R. Arkhipov, M. Arkhipov, A. Demircan, U. Morgner, I. Babushkin, N. Rosanov. Opt. Express, **29**, 10134–10139502 (2021).
[37] M. Arkhipov, R. Arkhipov, I. Babushkin, N. Rosanov. Phys. Rev. Lett., **128**, 203901 (2022).
[38] O. Diachkova, R. Arkhipov, A. Pakhomov, N. Rosanov. Opt. Commun., **565**, 130666 (2024).
[39] R. Arkhipov, A. Pakhomov, O. Diachkova, M. Arkhipov, N. Rosanov. Opt. Lett., **49** (10), 2549 (2024).
[40] R. Arkhipov, A. Pakhomov, O. Diachkova, M. Arkhipov, N. Rosanov. JOSA B, **41** (8), 1721 (2024).
[41] R.M. Arkhipov, O.O. D'yachkova, M.V. Arkhipov, A.V. Pakhomov, N.N. Rosanov. Opt. i spektr., **132** (9), 919 (2024) (in Russian).
[42] R.M. Arkhipov, O.O. Diachkova, M.V. Arkhipov, A.V. Pakhomov, N.N. Rosanov. JETP Lett., **121** (7), 520 (2025).
[43] R.M. Arkhipov, M.V. Arkhipov, A.V. Pakhomov, O.O. Diachkova, N.N. Rosanov. Bulletin of the Russian Academy of Sciences: Physics, **89** (1), 63–70 (2025).
[44] O. Diachkova, M. Arkhipov, N. Rosanov, R. Arkhipov. JOSA B, **42** (7), 1407 (2025).
[45] R. Arkhipov, M. Arkhipov, N. Rosanov. Opt. Lett., **50** (16), 4914 (2025).
[46] A. Yariv. *Quantum Electronics* (John Wiley & Sons, N.Y., London, Toronto, 1975).
[47] A. Taflov, S. Hagness. *Computational electrodynamics* (Artech house, 2000).
[48] O.D. Mücke, T. Tritschler, M. Wegener, U. Morgner. Phys. Rev. Lett., **87** (5), 057401 (2001).
[49] S. Nandi, E. Olofsson, M. Bertolino, S. Carlström, F. Zapata, D. Busto, C. Callegari, M. Di Fraia, P. Eng-Johnsson, R. Feifel, G. Gallician, M. Gisselbrecht, S. Maclot, L. Neoričić, J. Peschel, O. Plekan, K.C. Prince, R.J. Squibb, S. Zhong, P.V. Demekhin, M. Meyer, C. Miron, L. Badano, M.B. Danailov, L. Giannessi, M. Manfredda, F. Sottocorona, M. Zangrando, J.M. Dahlström. Nature, **608**, 488 (2022).
[50] A. De las Heras, C. Hernández-García, J. Serrano, A. Prodanov, D. Popmintchev, T. Popmintchev, L. Plaja. Phys. Rev. Research, **7** (2), 023268 (2025).
[51] R.M. Arkhipov, O.O. D'yachkova, P.A. Belov, M.V. Arkhipov, A.V. Pakhomov, N.N. Rozanov. ZhETF, **166** (8), 162 (2024). (in Russian).
[52] N.V. Vysotina, N.N. Rosanov, V.E. Semenov. Opt. Spectrosc., **106**, 713 (2009).
[53] J. Eschner, G. Morigi, F. Schmidt-Kaler, R. Blatt. J. Optical Society of America B, **20** (5), 1003–1015 (2003).
[54] D.D. Yavuz, N.R. Brewer, J.A. Miles, Z.J. Simmons. Phys. Rev. A, **88** (6), 063836 (2013).
[55] P. Borri, W. Langbein, J. Mørk, J.M. Hvam, F. Heinrichsdorff, M.H. Mao, D. Bimberg. Phys. Rev. B, **60**, 7784 (1999).
[56] L. Allen, J.H. Eberly. *Optical resonance and two-level atoms* (Wiley, N.Y., 1975).
[57] R.M. Arkhipov, M.V. Arkhipov, I. Babushkin, A. Demircan, U. Morgner, N.N. Rosanov. Opt. Lett., **41**, 4983 (2016).
[58] R.M. Arkhipov, M.V. Arkhipov, I. Babushkin, A. Demircan, U. Morgner, N.N. Rosanov. Sci. Rep., **7**, Art. No. 12467 (2017).
[59] R. Arkhipov, A. Pakhomov, M. Arkhipov, I. Babushkin, A. Demircan, U. Morgner, N.N. Rosanov. Sci. Rep., **11**, Art. No. 1961 (2021).
[60] R. Arkhipov, M. Arkhipov, A. Pakhomov, O. Diachkova, N. Rosanov. Phys. Rev. A, **109**, 063113 (2024).
[61] I.D. Abella, N.A. Kurnit, S.R. Hartmann. Phys. Rev., **141**, 391 (1966).
[62] E.I. Shtyrkov, V.S. Lobkov, N.G. Yarmukhametov. JETP Lett., **27** (12), 648 (1978).
[63] E.I. Shtyrkov, N.L. Nevelskaya, V.S. Lobkov, N.G. Yarmukhametov. Phys. Stat. Sol. B, **98** (2), 473–485 (1980).
[64] W. Babbitt, T. Mossberg. Opt. Commun., **65**, 185–811 (1988).
[65] A.C. Riis-Jensen, M.N. Gjerding, S. Russo, K.S. Thygesen. Phys. Rev. B, **102**, 201402 (2020).
[66] M. He, J. Cai, H. Zheng et al. Nat. Mater., **23**, 224–229 (2024).
[67] Q.H. Wang, K. Kalantar-Zadeh, A. Kis, J.N. Coleman, M.S. Strano. Nature Nanotechnology, **7** (11), 699–712 (2012).
[68] S. Zhang, S. Guo, Z. Chen, Y. Wang, H. Gao, J. Gómez-Herrero et al. Chem. Soc. Rev., **47** (3), 982–1021 (2018).
[69] M.V. Kovalenko, L. Protesescu, M.I. Bodnarchuk. Science, **358** (6364), 745–750 (2017).
[70] J. Ryou, Y.S. Kim, K.C. Santosh, K. Cho. Sci. Rep., **6** (1), 29184 (2016).
[71] L. Yuan, W. Hu, H. Zhang, L. Chen, Q. Wang. Front. Bioeng. Biotechnol., **8**, 21 (2020).
[72] P.C. Wu, T.H. Kim, A. Suvorova, M. Giangregorio, M. Saunders, G. Bruno, A.S. Brown, M. Losurdo. Small, **7** (6), 751–756 (2011).
[73] R.G. Arkhipov. Kvantovaya Elektron., **55** (5), (324) (2025) (in Russian).

Translated by J.Savelyeva